

# Fracture Process in Silicate Composite Specimens – X-ray Dynamic Observation and Numerical Modelling

Daniel Vavřík<sup>1,2,a</sup>, Tomáš Fíla<sup>2,b</sup>, Ivan Jandejsek<sup>2,c</sup>, Václav Veselý<sup>3,d</sup>,  
Petr Frantík<sup>3,e</sup>, Zbyněk Keršner<sup>3,f</sup>

<sup>1</sup>Institute of Theoretical and Applied Mechanics AS CR v. v. i., Prosecka 76, Prague 9,  
Czech Republic

<sup>2</sup>Czech Technical University in Prague, Institute of Experimental and Applied Physics, Horska  
3a/22, Prague 2, Czech Republic

<sup>3</sup>Brno University of Technology, Faculty of Civil Engineering, Institute of Structural Mechanics,  
Veveří 331/95; 602 00, Brno; Czech Republic

<sup>a</sup> vavrik@itam.cas.cz, <sup>b</sup> jandejs@itam.cas.cz, <sup>c</sup> fila@itam.cas.cz, <sup>d</sup> vesely.v1@fce.vutbr.cz,  
<sup>e</sup> kitnarf@centrum.cz, <sup>f</sup> kersner.z@fce.vutbr.cz

**Keywords:** Cementitious composite, Quasi-brittle fracture, Fracture process zone, Digital radiography, Computed tomography, Digital Image Correlation.

**Abstract.** Tensile failure in quasi-brittle materials is connected with formation and evolution of what is referred to as the Fracture Process Zone (FPZ) at the tip of propagating crack. Not only the very existence of the material damage area but also its descriptive parameters (volume, shape and energy dissipation distribution) have to be identified in order to validate approaches on both numerical modelling of quasi-brittle behaviour and experimental determination of fracture properties. Radiographic techniques and Digital Image Correlation method are used in the presented research as being very appropriate for analysing of the FPZ evolution during specimen loading. The experimental results are accompanied with predictions of the FPZ size and shape via semi-analytical technique serving as a part of developing comprehensive method for evaluation of the real fracture-mechanical characteristics of quasi-brittle materials from records of loading tests on laboratory-sized specimens.

## Introduction

The field of determination of characteristics of quasi-brittle building materials (most commonly cementitious composites) which should describe their ability to resist the fracture propagation has been thoroughly researched for several decades [1],[2],[3],[4]. However, some aspects that can be considered as crucial are still among the topics of intensive research. Effects of the size and geometry of the test specimen [5] regarded also as the effect of the specimen free boundaries [6],[7] seems to be the most relevant. An approach incorporating the parameters of the zone of material failure developing at the propagating macroscopic crack tip (fracture process zone, FPZ) has been proposed and (partially) employed recently [8]. The development of this approach is motivated by capturing of the above-mentioned effects in order to provide values of the fracture-mechanical parameters of the tested material independent of these effects. This methodology works with the reconstruction of the current size and shape of the FPZ (and perhaps also the intensity of the cohesive behaviour over the FPZ volume) [9] to which the amount of energy dissipated during the current step of fracture process should be related.

The development of the methodology is in a stage of testing, verification by numerical simulations [10],[11] and experimental validation [12] at present. It has to be emphasized that sound experimental evidence the FPZ size and shape (and possibly other characteristics) is published rather rarely. Techniques based on acoustic emission ([13],[14],[15],[16]), holographic interferometry, X-ray imaging (in combination with Digital Image Analysis – [17]) and infrared thermography were reported to be used to determine the FPZ in quasi-brittle materials (summarized e.g. in [3],[2]). Investigation of the material failure employing X-ray imaging is presented in this paper. Notched beams prepared from silicate-based composite were loaded in three point bending in a specially designed loading device. Crack length and FPZ shape/size during loading were analyzed using Digital Transmission Radiography and X-ray Computed Tomography (XCT). Visualization of the FPZ was enabled using tools of the Digital Image Correlation (DIC) method.

## Experiments

**Tested material and specimens.** The radiographic investigations of the material failure have limits in the dimensions of the test specimens. In our case, the length of the beam subjected to three point bending is limited by the chamber diameter of the loading device in which the specimen was placed. As a material for the specimen preparation, a fine-grained cementitious composite was chosen to simulate the failure process of normal-sized building structures/structural members made of concrete. Commercial dry plaster mix with maximum aggregate size equal to 1.2 mm (limestone debris) was selected. The bonding agent of this mix consists of both cement and calcium hydroxide. Minimal value of modulus of rupture quoted by the producer is 0.7 MPa. The mix was prepared according to the producer’s instructions.

The presented experiment was made as a pilot test to develop appropriate methodology of the FPZ and crack analysis intended for future experimental campaign. Series of 9 specimens were casted into the moulds: Specimen height  $W$  and length  $L$  are equal to 40 and 150 mm, respectively; three specimens’ breadths  $B$  (12, 20 and 30 mm) were selected; three different notch lengths  $a$  (4, 10 and 16 mm) were taken into account for each specimen breadth  $B$ . The notches were cut using diamond saw after demoulding. It provides the relative notch length  $\alpha = a/W$  equal to 0.1, 0.25 and 0.4. From this series the specimen with breadth  $B = 20$  mm and notch length  $a = 10$  mm was selected for the pilot test and is presented hereafter. The loading span  $S$  of the test geometry was set to 120 mm. Schematic picture of the specimen and related bending test is depicted in Fig. 1.

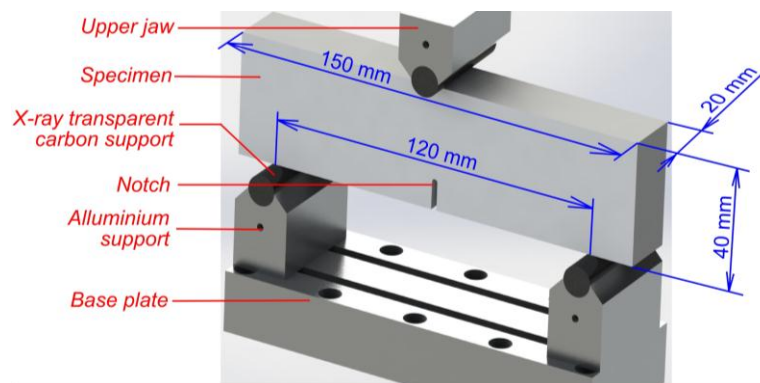


Fig. 1: Three point bending geometry; indication of dimensions of the specimen

**Instrumentation.** The modular tomographic system [18] provides an experimental setup allowing positioning adjustment of the X-ray tube, motorized positioning of the detector and the operational movement of the observed object fixed on a motorized stage. The linear axis of this stage enables to

set the projective magnification of the object. The rotation axis is used for tomographic data acquisition. The setup is equipped by the motorized revolver holder of the filters used for the fully automated acquisition of data needed for beam hardening correction, using the Signal to Equivalent Thickness (SET) method [19].

Hamamatsu microspot tube is employed as X-ray source in the tomographic system. This tube has a  $5\ \mu\text{m}$  spot size and cone beam. The pixelated Hamamatsu flat panel was utilized as X-ray imager in our work. This detector has active area  $120 \times 120\ \text{mm}$  with  $50\ \mu\text{m}$  pixel size. Binning of  $2 \times 2$  pixels was used in our work, so effective pixel pitch was equal to  $0.1\ \text{mm}$ .

Highly stiff loading compressive device was used for the specimen loading. This device allows very low loading velocity while it's relatively low weight and dimensions enable X-ray observation of the specimen in the radiographic cabin. Loading device generally consists of the actuating part and of the chamber in which specimen is placed. This chamber was manufactured from two parts. Top one is from the Certal aluminium alloy and bottom one from the  $0.6\ \text{mm}$  thick carbon epoxy laminate, which is practically transparent for X-rays. These parts are connected using bayonet mechanism. Support pins of the bending mechanism were also prepared from the carbon material. This solution enables radiographic observation of the analyzed specimen without any influence of the loading device for X-ray measurement. Whole setup is depicted in Fig. 2 left. Disassembled chamber with the specimen is in Fig. 2 right.

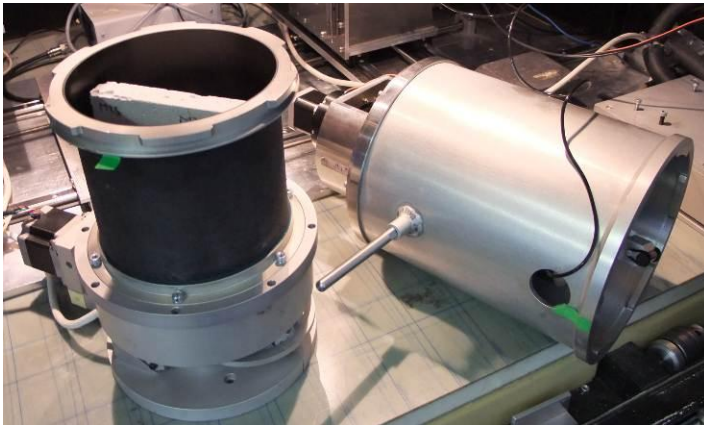


Fig. 2: Radiographic/mechanical test setup: disassembled chamber with the specimen (left); completely arranged testing device (right)

**Test procedure details.** Specimen was loaded with velocity  $0.1\ \mu\text{m}/\text{min}$  (that holds true for the displacement imposed by the engine of the loading device,  $d_{\text{eng}}$ , which is not equal to the mid-span deflection of the tested beam,  $d$ ). Exposure time of one X-ray radiogram was  $5 \times 0.48$  seconds (it corresponds to the  $0.5\ \mu\text{m}$  displacement increment due to read out time).

These radiograms were recorded continuously during loading while CT measurement was done in two load levels. For the CT measurement, 240 snapshots ( $180^\circ$  rotation) were taken. Total time of one CT measurement was 50 minutes. The specimen rotation axis was at a distance of  $188\ \text{mm}$  from the X-ray tube spot and the flat panel was at distance  $429\ \text{mm}$  from the tube spot. Therefore, the pro-

jected magnification was 2.3. The X-ray tube was operated at 80 kV and 125  $\mu$ A. CT reconstruction was done considering divergent X-ray beam [20].

**Results.** It is clearly visible from load–displacement diagram (LD diagram) plotted in Fig. 3a) that the used loading device enables to study processes with very high loading precision. Measured force  $P$  as a function of both the displacement imposed by the engine  $d_{eng}$  and the estimation of the real deflection of the beam  $d$  (without displacements taken place at the contacts of the loading chain parts and the push-in of supports into the specimen) is showed. The real displacement  $d$  was not measured directly, it was determined from optical measurements using DIC.

The radiogram of the specimen taken 1.5  $\mu$ m after surpassing maximal loading force (point A in LD diagram) is in Fig. 3b) (only middle part of the specimen is showed, overturned upside down). Significant internal structure can be observed, which corresponds to the material inhomogeneity. It is almost impossible to observe FPZ directly in the investigated specimen due to this structure.

DIC tools were used to avoid this difficulty; the actual and initial radiograms were subtracted (resulting in subtraction image) to find changes of the specimen density considering specimen movement during its loading. Such image are shown in Fig. 3c) (three blue diamond shape spots occurred due to the flat panel local noise, one of them in the middle of the crack path, unfortunately). It is apparent that FPZ has significant role for the fracture mechanics description. In the initial stages of the fracture process the crack is much shorter than FPZ (e.g. in the case of stage A, the FPZ length is estimated to 0.7 mm, the FPZ length to 6.5 mm) as is evident from first row (and left column) of in Fig. 4.

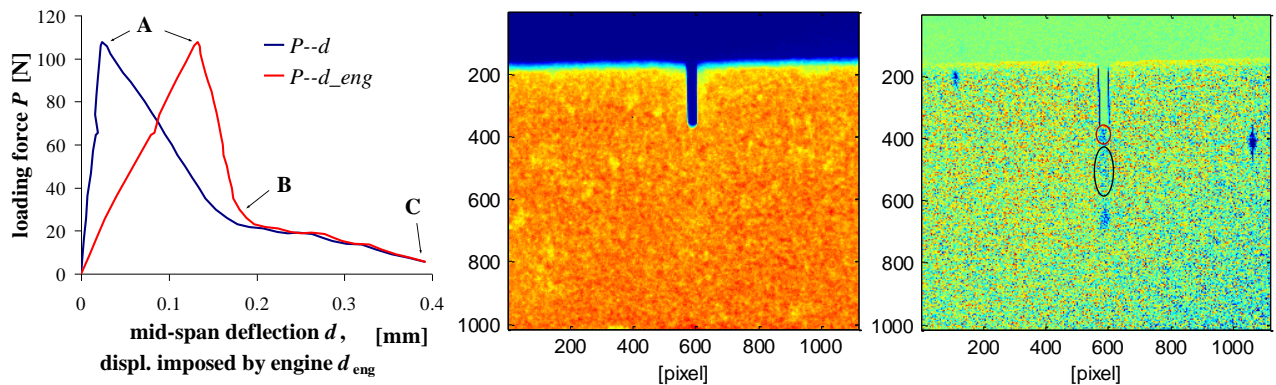


Fig. 3: a) Load–deflection diagram with indication of stages in which FPZ zone was investigated (in B and C also using CT); b) radiogram of the middle part of the specimen taken at the maximum load; note that FPZ is not visible due to significant variation of the material density; c) subtraction image shows colours corresponding to the material effective density (averaged through the specimen thickness); the crack and the FPZ can be estimated (surrounded by red and black ellipse, respectively) are visible, the radiogram pixel size is 44  $\mu$ m

The subtraction images at loading stages B and C are shown in the subsequent rows in Fig. 4. The CT measurement were done at these fracture process stages. It was proven that subtraction image (comparing with CT measurement) can describe the crack front position and the FPZ shape/size which is represented by the significant change of the specimen density, although the boundary between the crack tip and the FPZ is quite blurred. Crack and FPZ lengths were estimated to 2.7 and 16 mm, respectively, at stage B. At stage C, the crack was 17 mm long and practically whole remaining ligament was weakened by the FPZ.

As was mentioned above, CT measurement was done in two loading levels (points B and C in LD diagram). Vertical cross-section of the CT reconstruction at loading level B is depicted in Fig. 5, first row and left column. This cross-section lies in the centre of the notch. It is visible, that speci-

men is damaged preferentially in the specimen's centre. Virtual hole in the middle came from the flat panel local noise. Magistral crack tips are imaged in Fig. 5 right (correspond to the slice number 155 and 440 at cross-section left for stage B and C, respectively. Magistral crack tips are emphasized by blue ellipses). These crack tips in the same position as in subtraction image, Fig. 4 left.

### Free crack length and FPZ size/shape estimates

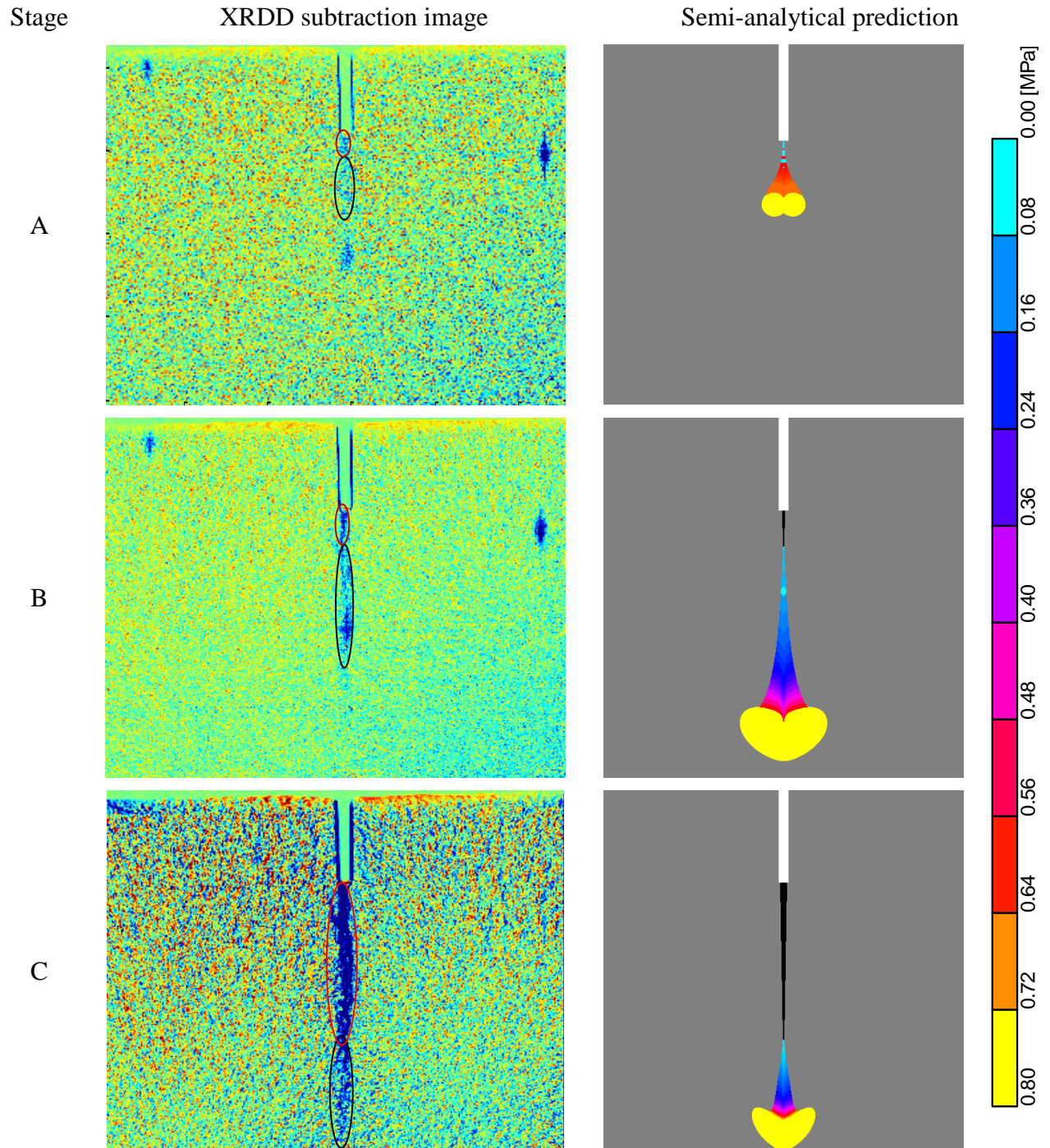


Fig. 4. Subtraction images at the fracture process stages A, B, C (left); corresponding estimates of the FPZ size/shape (with indication of the cohesive stress level over its volume – see the scale) and free crack lengths (black) using the semi-analytical technique (right).

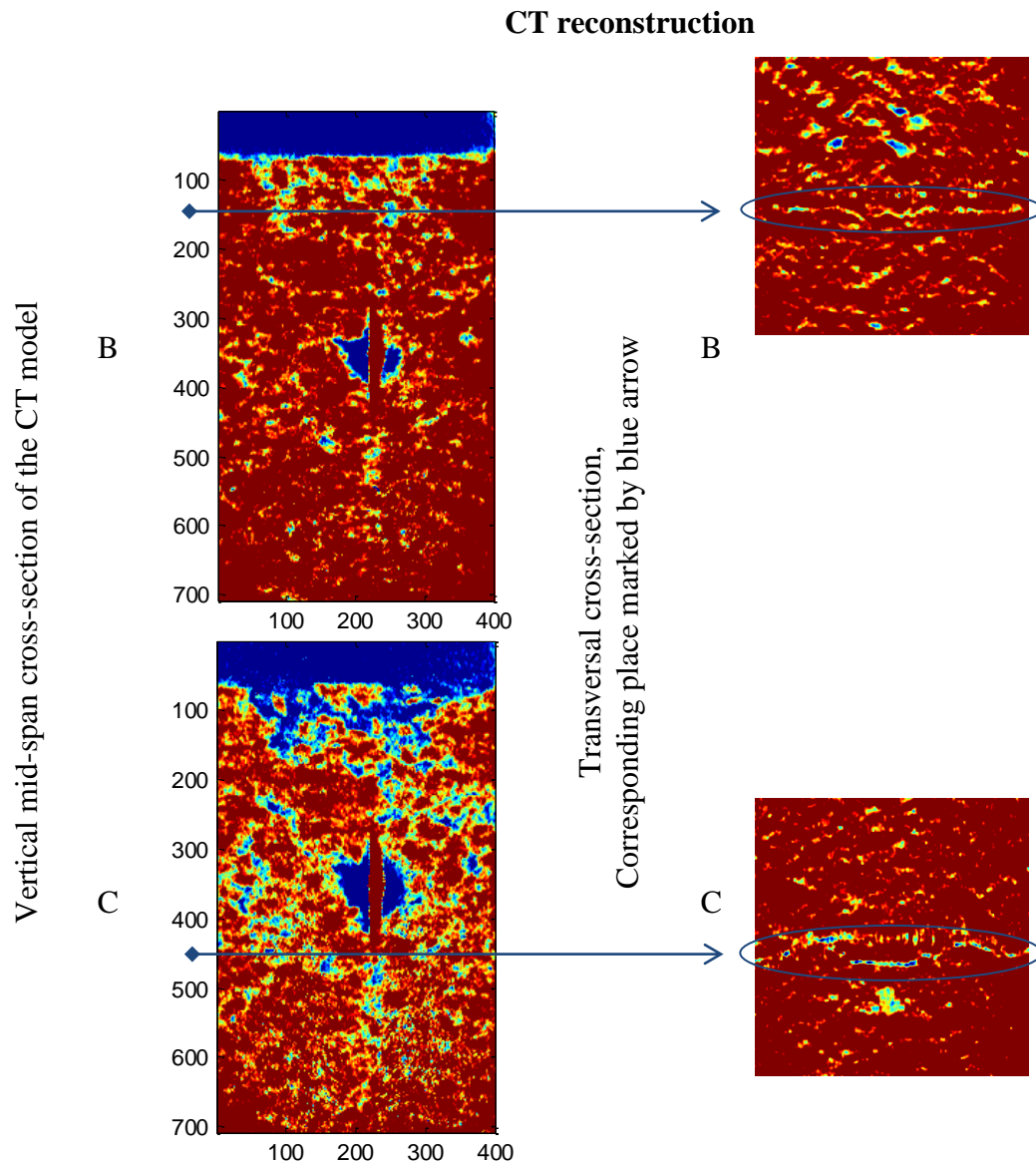


Fig. 5: CT reconstruction of the specimen at loading levels B and C: Vertical CT cross-section which corresponds to the plane in the centre of the notch (left); tip of macroscopic (transversal) crack (surrounded by blue ellipse) (right)

Generally, crack does not follow straight direction and its front is not sharp as it is possible to document using CT reconstruction. It is hard to distinguish which individual voids were born during loading and which were presented from the beginning. However it can be shown, that void density is significantly increasing during loading as presented in Fig. 6 using 3D visualization, stage B left, stage C right. Only central part of the specimen containing crack was selected for this visualisation.

### Modelling – fracture test reconstruction

The used method for estimation of the FPZ extent is based on three fundamental approaches to model material failure. It exploits the theory of linear elastic fracture mechanics (LEFM), classical nonlinear fracture models for concrete, i.e. the effective crack model (ECM, [1]) and the fictitious crack model (FCM, [21]), and plasticity theory. For the general description of the stress field in cracked bodies, more terms of the Williams power series [22] are taken into account. A detailed description of the method of the FPZ extent estimation is given in [9],[8].

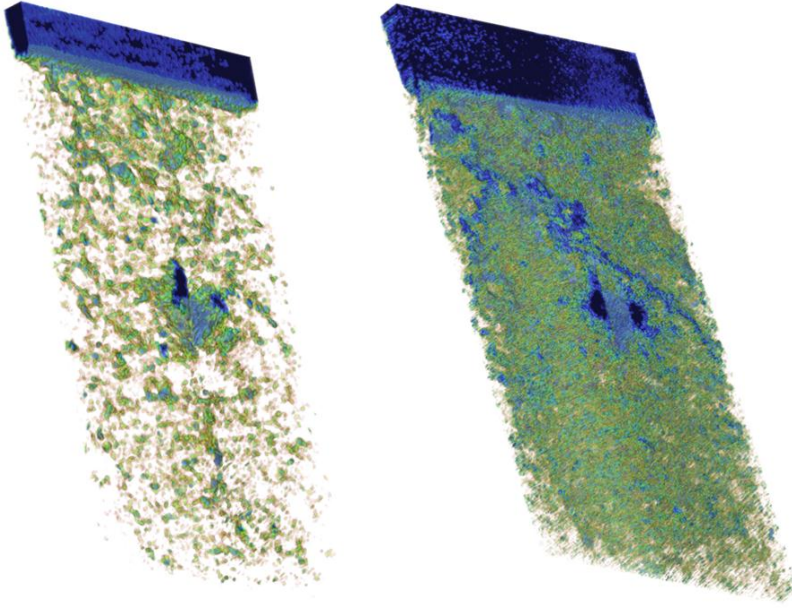


Fig. 6: 3D visualisation of the voids at loading level B left and C right; it is visible that these voids and consequent macroscopic crack are preferentially occurring in the middle of the specimen

The method is utilized within the processing of fracture test records; typically, the LD diagrams. For individual stages of the fracture process (i.e. points in the LD diagram), the length of the equivalent elastic crack is estimated by means of the ECM. Then, the stress state in the body with the effective crack is approximated through the Williams power series. Subsequently, the extent of the zone where the until-now elastic material starts to fail is determined by comparing the tensile strength  $f_t$  of the material to a relevant characteristic of the stress state around the crack tip (some sort of equivalent stress,  $\sigma_{eq}$ , for cementitious composites e.g. the Rankine or Drucker-Prager failure criterion can be employed).

This zone referred to as  $\Omega_{PZ}$  (index PZ stands for Plastic Zone). Then, in agreement with the cohesive crack approach, the FPZ (marked as  $\Omega_{FPZ}$ ) is supposed to extend from the  $\Omega_{PZ}$  around the current crack tip up to an  $\Omega_{PZ}$  corresponding to the prior crack tip (i.e. currently a point at the crack faces), where the value of crack opening displacement  $w$  reaches its critical value  $w_c$  (i.e. the value of cohesive stress  $\sigma(w)$  drops to zero here). Thus, the region  $\Omega_{FPZ}$  is assembled as a union of  $\Omega_{PZ}$  within the field of activity of the cohesive stress. In order to project the shape of the cohesive stress function  $\sigma(w)$  into the shape of the  $\Omega_{FPZ}$ , the individual plastic zones  $\Omega_{PZ,i}$  creating the entire FPZ are scaled by a factor of  $\sigma(w_i)/f_t$  in this method.

The LD diagram shown in Fig. 3a) is used as input into the technique for the estimation of the FPZ extents. Other necessary inputs into the procedure are following: 4 terms of the Williams series, Rankine failure criterion, values of tensile and compressive strengths  $f_t$  and  $f_c$  (estimated for the tested composite as) equal to 0.8 MPa and 4.0 MPa, respectively, value of fracture energy  $G_f$  equal to  $20 \text{ Jm}^{-2}$  (determined from the recorded LD diagram), and the exponential (Hordijk's) cohesive function. The FPZ extents (including the indication of the cohesive stress distribution – from yellow colour corresponding to  $f_t$ , to cyan corresponding to zero cohesive stress) in 3 stages of the fracture process corresponding to those in which the detailed radiographic analysis was conducted (A, B, C) are shown in the right column in Fig. 4). Note that the value of the cohesive stress is inversely proportional to the amount of energy dissipated for the fracture: In the yellow parts of the FPZ (the largest ones) the cohesive stress is highest; however, lowest amount of energy is released in the failure mechanisms. In contrast, at the tails of the FPZ (cyan) the maximal energy release is observed.

## Conclusions

It was proven that X-ray radiography in conjunction with Digital Image Correlation and CT reconstruction are powerful tools for analysing of the crack and FPZ evolution during quasi-brittle specimen loading.

Experimental results showed that FPZ is for the tested material and specimen size significant in comparison with the macroscopic crack length. Moreover, crack does not follow straight direction and its front is not sharp. It can be concluded from these reasons that linear fracture mechanics based on assumption of the continuum material can't describe such crack behaviour.

Results of the semi-analytical procedure for the FPZ extent estimation is compared with the experimental data. Agreement in some aspects was obtained, however, further research is needed (regarding e.g. the interpretation of the energy dissipation etc.). The present type of analysis is planned to be performed on various specimen sizes and test geometries in near future.

**Acknowledgements:** Financial support from the Czech Science Foundation, project No. P105/11/1551, and ITAM CET RVO: 68378297 are gratefully acknowledged. Material for specimens preparation was granted by PROFI am BAU CM, spol. s r.o. (Ernstbrunner Kalktechnik GmbH).

## References

- [1] B.L. Karihaloo: *Fracture mechanics and structural concrete* (Longman Scientific & Technical, New York 1995).
- [2] S.P. Shah, S.E. Swartz, C. Ouyang: *Fracture mechanics of structural concrete: applications of fracture mechanics to concrete, rock, and other quasi-brittle materials* (John Wiley & Sons, Inc., New York 1995).
- [3] J.G.M. van Mier: *Fracture processes of concrete: Assessment of material parameters for fracture models* (CRC Press, Inc., Boca Raton 2007).
- [4] Z.P. Bažant, J. Planas: *Fracture and size effect in concrete and other quasibrittle materials* (CRC Press, Boca Raton 1998).
- [5] Q. Yu, J.-L. Le, C.G. Hoover, Z.P. Bažant: *J Engrg Mech (ASCE)*, 136(1) (2010).
- [6] X.-Z. Hu, K. Duan: *Engrg Fract Mech* 74 (2007), p. 1093.
- [7] K. Duan, X.-Z. Hu, F.H. Wittmann: *Mechanics of Materials*, 38 (2006), p. 128.
- [8] V. Veselý, P. Frantík, Z. Keršner in: *Proc. of conf. CC 2009*, Funchal, Portugal. B.H.V. Topping, L.F. Costa Neves, R.C. Barros (eds.) (Civil-Comp Press, UK 2009), paper 194.
- [9] V. Veselý, P. Frantík, P.: *Applied and Computational Mechanics* 4 (2010), p. 237.
- [10] P. Frantík, V. Veselý, Z. Keršner in: *Proc. of the 2nd Int. Conf. on Parallel, Distributed, Grid and Cloud Computing for Engineering*, Ajaccio, France. P. Iványi and B.H.V. Topping (eds.) (Civil-Comp Press, UK 2011), paper 62.
- [11] P. Frantík, V. Veselý, Z. Keršner: submitted to *Comp Struct*, 2011.
- [12] V. Veselý, Z. Keršner, J. Němeček, P. Frantík, L. Řoutil, B. Kucharczyková: *Chem. Listy* 104 (2010), p. 382.
- [13] S.P. Shah: *Engrg. Fract. Mech.* 35 (1990), p. 3.
- [14] K. Otsuka, H. Date, H.: *Engrg. Fract. Mech.* 65 (2000), p. 111.
- [15] H. Mihashi, N. Nomura: *Nuclear Engineering and Design* 165 (1996), p. 359.
- [16] S. Muralidhara, B.K. Raghu Prasad, H. Eskadri, B.L. Karihaloo: *Constr Build Mat* 24 (2010), p. 479.
- [17] I. Jandejsek, F. Nachtrab, N. Uhlmann, D. Vavřík: *NIM A*, Vol. 6 (2011), p. 185, doi:10.1016/j.nima.2010.06.162.
- [18] J. Jakůbek, D. Vavřík, T. Holý, M. Jakůbek, Z. Vykydal: *NIM A*, Vol. 563, Issue 1 (2006), p. 278, doi:10.1016/j.nima.2006.01.033.
- [19] D. Vavřík: *NIM A*, Volume 633, Supplement 1, May 2011, (2011), p. 152, doi:10.1016/j.nima.2010.06.160.
- [20] D. Vavřík, P. Soukup: *JINST\_007P\_1011* (2011), doi:10.1088/1748-0221/6/11/C11034.
- [21] A. Hillerborg, M. Modéer, P.-E. Petersson: *Cem Concr Res*, 6 (1976), p. 773.

[22] M.L. Williams: ASME J. Appl. Mech., 24 (1957), p. 109.